ADVANCED INTELLIGENT SYSTEMS
Open Access
www.advintellsyst.com

Propulsion of Planar V-Shaped Microswimmers in a Conically Rotating Magnetic Field

Yasin Cagatay Duygu, U Kei Cheang, Alexander M. Leshansky, and Min Jun Kim**

Planar magnetic microswimmers bear great potential for in vivo biomedical applications as they can be mass-produced at minimal costs using standard photolithography techniques. Therefore, it is central to understand how to control their motion. This study examines the propulsion of planar V-shaped microswimmers in an aqueous solution powered by a conically rotating magnetic field and compares the experimental results with theory. Propulsion is investigated upon altering the cone angle of the driving field. It is shown that a V-shaped microswimmer magnetized along its symmetry axis exhibits unidirectional in-sync propulsion with a constant (frequency-independent) velocity in a limited band of actuation frequencies. It is also demonstrated that the motion of individual and multiple in-plane magnetized planar microswimmers in a conically rotating field can be efficiently controlled.

1. Introduction

The propulsion of robotic microswimmers that can be controllably steered through complex fluidic environments has recently garnered significant attention. In vivo biomedical applications of microrobotics include drug delivery, minimally invasive surgery, cell therapy, in situ sensing, and tissue engineering.[1–4] Emerging techniques for microswimmer actuation include magnetic actuation, thermal actuation, light, and ultrasound, as well as nanowires and Janus particles that are catalytically driven.[5–7] Magnetic actuation is a highly promising technique that offers remote, engineless, and fuel-free actuation. While the conventional techniques rely on magnetic fields with a strong gradient to generate force to remotely steer magnetic micro/nanoparticles,[8,9] alternative methods rely on relatively weak uniform rotating magnetic fields that apply torque on specially shaped magnetic microswimmers resulting in their rotation and linear motion owing to rotation-translation coupling. Although a gradient field can pull an isotropic (i.e., spherical) particle, it is not a particularly effective method because of the high magnitude of the magnetic field necessary to create a discernible field gradient at the (sub)micron length scale of the particle.[9,10]

Swimming characteristics of microorganisms and biologically inspired magnetic microswimmers at low-Reynolds-number have been studied for over 50 years.[1,11–13] Various geometries have been investigated for microscale propulsion including helical, spiral-shaped microswimmers that were explored in detail both theoretically and experimentally.[14–18] However, manufacturing of these structures is complex and expensive, requiring the use of sophisticated procedures, such as delamination of magnetic stripes, glancing angle deposition, direct laser writing, biotemplated synthesis using biological spiral organelles, and two-photon polymerization of a curable magnetic polymer composite or spiraling microfluidic flow lithography.[19–26]

It has been shown theoretically that achiral geometries offer comparable performance to chiral (helical) propeller designs.[27,28] The theory of magnetically driven propulsion of an arbitrarily shaped microswimmer[29] suggests that chirality is not a purely geometric property, but could also depend on magnetization, for example, rendering geometrically achiral microswimmer effectively chiral for a particular orientation of the magnetic moment.[30] Additionally, it has been demonstrated with spherical microbeads that nonlinear rheology of the suspending fluid can induce symmetry breaking and enable

Y. C. Duygu, M. J. Kim
Department of Mechanical Engineering
Southern Methodist University
Dallas, TX 75204, USA
E-mail: mjkim@lyle.smu.edu

U K. Cheang
Department of Mechanical and Energy Engineering
Southern University of Science and Technology
Shenzhen 518055, China

U K. Cheang
Shenzhen Key Laboratory of Biomimetic Robotics and Intelligent Systems
Southern University of Science and Technology
Shenzhen 518055, China

U K. Cheang
Guangdong Provincial Key Laboratory of Human-Augmentation and Rehabilitation Robotics in Universities
Southern University of Science and Technology
Shenzhen 518055, China

A. M. Leshansky
Department of Chemical Engineering
Technion - Israel Institute of Technology
Haifa 32000, Israel
E-mail: lisha@technion.ac.il

The ORCID identification number(s) for the author(s) of this article can be found under https://doi.org/10.1002/aisy.202300496.

DOI: 10.1002/aisy.202300496

rotation-translation coupling.[31,32] Despite recent theoretical advances in comprehending the driven propulsion of planar magnetic microswimmers, there is no systematic experimental investigation testing the role of geometry, magnetization, or field frequency and configuration, other than the experiment with the upscaled (cm-sized) 3D-printed propellers by Sachs et al.[30] The use of planar microswimmers, which can be mass-produced through standard photolithography, is an attractive option in the field of microrobotics due to its ease of fabrication and potential for scalability and biocompatibility.[33,34]

Planar magnetic microswimmers are prone to magnetize in their plane, while in-plane magnetized microswimmers typically exhibit bidirectional propulsion (i.e., parallel and antiparallel to the field-rotation axis) when driven by a standard in-plane rotating magnetic field.[29,30] Unidirectional propulsion requires an off-plane magnetization, which is a nontrivial undertaking. However, the controlled (unidirectional) propulsion of in-plane magnetized planar microswimmers can be achieved by adding a constant magnetic field along the field rotation axis, such that the resulting field vector tracks the envelope of the cone. Cohen et al. found that in a finite band of actuation frequency, a symmetric V-shaped planar microswimmer magnetized along its symmetry axis exhibits unidirectional propulsion with a constant (frequency-independent) velocity under a conically rotating field.[35] Tottori et al. experimentally demonstrated propulsion of the asymmetric planar L-shaped planar magnetic microswimmers in a conically rotating field, however, no theory was developed to elucidate the role of the magnetization, the field configuration, and frequency.[36]

In this study, the actuation of geometrically achiral planar microswimmers fabricated by photolithography is studied experimentally. Our research aims to systematically investigate their controlled (unidirectional) propulsion in a conically rotating magnetic field and to compare the experimental findings to the theoretical predictions.

2. Results and Discussion

2.1. Experimental Results

2.1.1. Microswimmer Dimensions, Actuation Scheme, and Problem Formulation

The microswimmers have a symmetric V-shape geometry with a central angle of 120 degrees. This particular choice of the planar geometry follows from the previous theoretical predictions, indicating that symmetric V-structures are nearly optimal for propulsion,[27] while the central angle of 120° maximizes the propulsion velocity.[35] The base of the structure is 40 μm long and 20 μm wide, while its height is 5 μm (height-to-width aspect ratio $h:w = 1:4$). All microswimmers are magnetized along their symmetry axis and magnetization orientation was verified using a static magnetic field prior to propulsion experiments. All the experiments are conducted under a uniform conically rotating magnetic field which is illustrated in **Figure 1**a. At the beginning of the experiment, the microswimmers are located at the bottom of the chamber surface due to gravity. If the microswimmers are allowed to stay long enough at the chamber bottom, they tend to adhere to the surface. The following method was employed to launch the microswimmers from the bottom of the chamber. This involved utilizing a sudden application of two magnetic fields rotating around the X and Z axes, respectively, followed by the application of a conically rotating field to propel the microswimmers upward. To eliminate the potential boundary effects in propulsion experiments, the microswimmers are first stirred upward to a minimum distance of ≈1000 μm above the bottom of the chamber. Another conically rotating magnetic field with a static field component acting in the XY-plane is then applied to propel the microswimmers along the Y-axis (parallel to the chamber bottom) and measure their propulsion velocity. Due to gravity, microswimmers sink during their propulsion, as illustrated

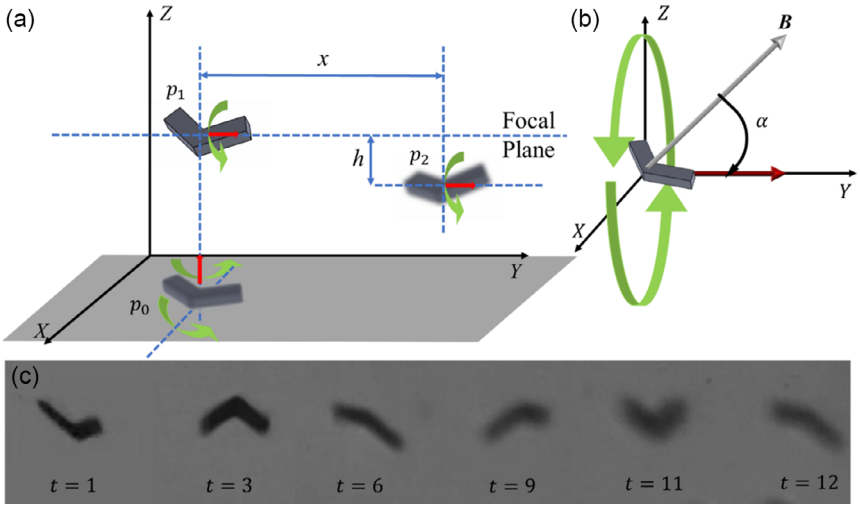

Figure 1. a) Illustration of propulsion of a planar microswimmer. p_0 shows the initial position at the bottom surface. Microswimmer reaches the position p_1 after swimming upward. p_2 is the final position after applying the conically rotating magnetic field. x shows the displacement due to propulsion; h marks the displacement due to gravitational settling. b) The conically rotating field, δ, and cone angle α are illustrated. The red arrow represents the static magnetic field, the green arrow illustrates the direction of the in-plane rotating field, and the conically rotating field (gray arrow) is the superposition of these two fields. c) Propulsion of an individual microswimmer in a conically rotating field at various instants$t$ (in seconds).

in Figure 1a and this gravitational settling causes the microswimmers to move away from the focal plane, resulting in blurry images, as shown in Figure 1c.

The conically rotating (around the *Y*-axis) magnetic field is given by:

$$B = B(\hat{x}\sin\omega t + \gamma\delta + \hat{z}\cos\omega t) \quad (1)$$

where $\alpha = \tan^{-1}(1/\delta)$ is the cone angle, B is its magnitude, ω is the angular frequency, and the hatted symbols stand for the unit vectors along the corresponding axes. As depicted in Figure 1b, the cone angle α is defined as the angle between the *Y*-axis of rotation and the direction of the resulting field $\boldsymbol{B}$. The superposition of an in-plane rotating field (green arrow) and a static field (red arrow) results in an instantaneous field vector $\boldsymbol{B}$, as depicted by the gray arrow in Figure 1b.

2.1.2. Propulsion of Individual and Multiple Microswimmers

Figure 1c depicts the propulsion of an individual microswimmer. A conically rotating field must be applied to the desired swimming direction to steer microswimmers. The direction of the static field (as well as the axis of the field rotation) is determined based on the vector between the microswimmer's desired and current positions. Based on the desired and current positions, the axis of rotation of the magnetic field is rotated about the *Z*-axis to steer microswimmers in any other direction in the *XY* plane.

Figure 2 demonstrates the controlled propulsion of a collection of three microswimmers. To steer a swarm of microswimmers, the current position is determined by selecting its average position. The trajectories of the individual microswimmers are depicted in Figure 2a, and their velocities throughout the experiment are calculated (Figure 2b). It can be readily seen that the swarm of microswimmers can be effectively steered similarly to an individual propeller, suggesting that their mutual magnetic and/or hydrodynamic interactions are negligible. Due to minor differences in the magnetization direction of each microswimmer, their velocities throughout the experiment are not identical. In this particular experiment, a conically rotating field with a frequency of 1.5 Hz and a rotating field component magnitude of 15 mT ($\delta = 0.1$) is applied. The static field causes a displacement due to a change in orientation, which leads to an increasing velocity at the start of the experiment. After the rotating field is turned off by the end of the video, there is a dramatic decrease in velocity, and propulsion ceases. Notice that while the velocity profiles of microswimmers 2 and 3 exhibit greater similarity, microswimmer 1 has a bit different velocity dependence probably due to a slightly different magnetization. Microswimmer 1 has an average velocity of 6.9 μm s^{-1}, while microswimmers 2 and 3 have average velocities of 8.2 and 7.4 μm s^{-1} during their steady propulsion, respectively.

Figure 3 illustrates the demonstrated capability of microswimmers to follow complex trajectories and exhibit swarm behavior. Predetermined trajectories in the shapes of the letters "**S**", "**M**", and "**U**" are shown in Figure 3a–c. For each of these three tests, a 25 mT rotational field with a frequency of 10 Hz was superimposed on a 7.5 mT static field ($\delta = 0.3$). To design the trajectories, we employed straight strokes, each of which consisted of a single continuous line segment. Five different strokes were involved to generate the trajectory "**S**" in Figure 3a. The axis of rotation (i.e., direction of the static field) was gradually rotated to change the propulsion direction. Before every directional change, only a static field was applied for one second. Figure 3d–f displays the magnitude of the propulsion velocity throughout the experiment for the letter "**S**", "**M**", and "**U**" trajectories. The position and velocity plots' color coding varies with time. The velocity of the microswimmer at the position corresponding to the color code utilized in the position plot depicted in Figure 3a–c is shown in Figure 3d–f.

The "**S**" trajectory consists of five distinct strokes along the *X* or *Y* axis. The constant velocity periods in Figure 3d also depict these strokes. There is a one-second delay between each stroke and the application of the next line's conically rotating field, resulting in a significant decrease in velocity after each stroke as can be seen in Figure 3d. During this one-second interval, only the static field for the following stroke was applied. The third stroke of "**S**" deviates slightly from what was intended because of the displacement in the *Y* axis. This displacement is caused by minor internal flow. The five strokes had average velocities of 39.0 μm s^{-1}, 42.1 μm s^{-1}, 47.3 μm s^{-1}, 45.2 μm s^{-1}, and 39.4 μm s^{-1}, resulting in an average velocity of 42.4 μm s^{-1} for the whole "**S**" trajectory.

Similarly, the "**M**" trajectory has four distinct strokes, as shown in Figure 3b. As shown in Figure 3e, there is also a one-second gap between applying the conically rotating field

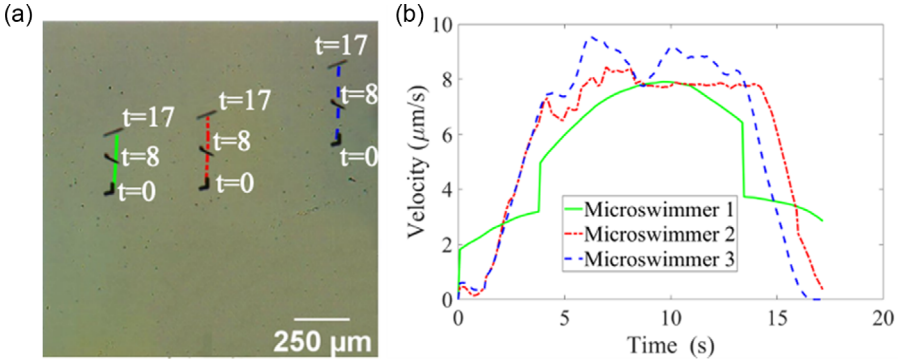

Figure 2. a) 2D trajectory of a collection of three microswimmers under a conically rotating magnetic field ($\delta = 0.1$). b) The velocity of the three microswimmers versus time of the experiment.

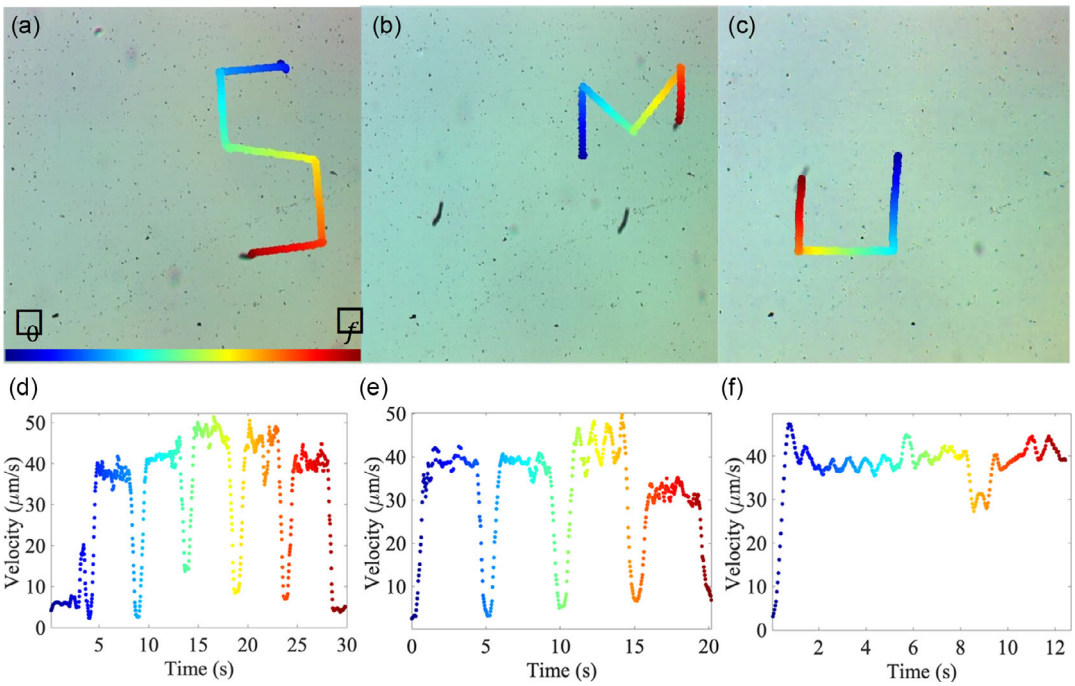

Figure 3. Results of preplanned trajectories in the shape of the letters: a) "**S**", b) "**M**", and c) "**U**". The time of the experiment is color-coded (see the color bar in (a)), while t_0 and t_f represent the initial and the final time, respectively. The microswimmers are at their final locations. d–f) The color-coded velocity magnitude of the microswimmers along their "**S**", "**M**", and "**U**" trajectories in (a), (b), and (c), respectively.

for these strokes, resulting in a velocity decrease. Due to the drift caused by the preceding rotation and the static field, the velocity during these one-second gaps does not reach precisely zero in Figure 3d,e. We track the displacement of the microswimmer's centroid to determine the position and velocity of microswimmers. The static field that is applied during the one-second pause alters the orientation of the microswimmer and causes a change in velocity due to the displacement of the centroid. The average velocity throughout all experiments was 38.1 μm s^{-1}. The average velocity of the four distinct strokes was 39.9 μm s^{-1}, 38.3 μm s^{-1}, 41.6 μm s^{-1}, and 32.5 μm s^{-1}. Due to the slight flow in the *Y* axis, which can be caused by a weakened bond between glass and polydimethylsiloxane (PDMS), the final stroke has a lower velocity, whereas the third stroke has a higher velocity magnitude.

The trajectory denoted by "**U**" comprises three strokes. To expedite the experiment, the one-second interval between these strokes is not utilized for trajectory "**U**". The average velocity of the three distinct strokes was 38.0 μm s^{-1}, 38.1 μm s^{-1}, and 37.6 μm s^{-1} with an overall mean velocity of 37.9 μm s^{-1} throughout the experiment. Except at the commencement of the last direction change, there was no significant change in velocity over time.

Controlling the motion of multiple microswimmers in a fluid environment is crucial for prospective in vivo and in vitro applications, such as targeted drug delivery. One significant advantage of our 2D microswimmers over other systems is the unidirectional propulsion with a constant speed over a range of actuation frequencies, as demonstrated experimentally. This characteristic provides a clear benefit in terms of controllability compared to 2D microswimmers that are powered by an in-plane rotating field and exhibit bidirectional propulsion with frequency-dependent velocity.[30] Additionally, the rapid mass fabrication by photolithography creates promising opportunities for swarm applications. Following this, **Figure 4**a shows the propulsion of a swarm of 13 microswimmers. The experimental chamber is subjected to a magnetic field rotating conically around the *Y*-axis. Identical and distant microswimmers are anticipated to propel along the *Y*-axis with equal velocities (see Figure 2a). It can be readily seen that some of the tracked

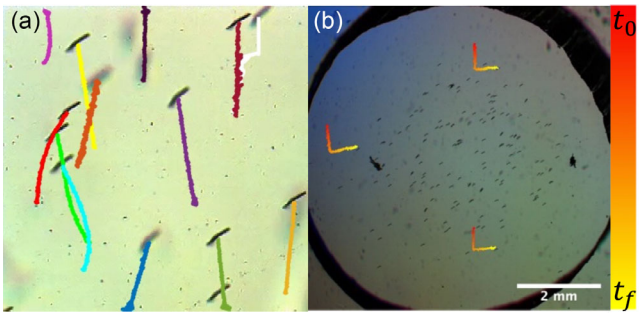

Figure 4. a) Motion of a swarm of microswimmers subjected to a conically rotating field. Different colors represent the individual trajectories of the microswimmers in the swarm and their final positions. b) Large swarm of microswimmers subjected to a conically rotating field moving along a preprogrammed "**L**" trajectory. The time of the experiment is color-coded (see the color bar on the right, where t_0 and t_f represent the initial and the final time, respectively). The scale bar size is 2 mm.

microswimmers, such as those marked orange, dark blue, and brown or yellow, purple, and dark green colors in Figure 4a, are swimming in the same direction with similar velocities. However, some microswimmers demonstrate subtle differences in their trajectories and velocities. The velocity differences could be a result of variations in the magnetization orientation and/or magnitude between microswimmers resulting from minor manufacturing defects. The trajectory distortion (i.e., deviation from the straight line parallel to the Y axis) could be a result of mutual hydrodynamic interactions between microswimmers. Each rotating propeller acts as a point rotlet[37] to the leading approximation, and induces a swirling flow in its vicinity. Although this swirling flow does not affect the relative motion of the microswimmers, it does deform their individual trajectories.[38] Due to the $\approx 1/r^2$ decay of this swirling flow, the dynamics of the adjacent microswimmers remains largely unaffected, provided that they are separated by a distance l greater than the propeller's own size.[38] In Figure 4a, the red, green, and cyan microswimmers maintain a consistent depth throughout the experiment. Given that their initial separation is $\approx l$, the mutual hydrodynamic interaction results in the observed distorted trajectories. Throughout the experiment, the minimal measured separation was $\approx$58 μm, while the microswimmer's size was $l \approx$89 μm. Notice that some microswimmers' trajectories (e.g., marked by dark red and white colors on the upper right corner of the figure) overlap in the XY-plane; however, their positions are well separated vertically. Despite observed deviations, in most scenarios with multiple microswimmers, velocity variations are minor. Thus, the velocity of a single microswimmer can represent that of a swarm. Figure 4b displays a larger swarm of microswimmers steering under a conically rotating field following a preprogrammed L-shaped trajectory. The corresponding video is provided in the Supporting Information. This setup was designed to elucidate the collective behavior in a more realistic setting. Each microswimmer is depicted at the final point of its respective trajectory. A gradient colormap on the right edge indicates the time progression along the trajectories of three microswimmers, serving as representative examples of the swarm's propulsion. The consistency in the microswimmers' trajectories emphasizes their potential toward realistic applications involving swarms. It also supports the notion that the dynamics of a single microswimmer studied in this article in detail, is representative of a swarm motion. Preplanned variance in either geometry and/or magnetization of individual propellers can be used to steer them differently under a global rotating magnetic field. For instance, Giltinan et al. demonstrated individual control by employing geometric variations in the microrobotic helices.[39]

2.1.3. The Effect of the Cone Angle on Propulsion

To understand the effect of the static field magnitude, which also varies cone angle α and δ (Figure 1b), a straightforward experiment is conducted, as shown in Figure 1a. Theoretically, there exists a finite band of in-sync actuation frequency, whereas the propulsion velocity remains constant for a fixed δ (i.e., cone angle). Moreover, the propulsion velocity in these frequency bands increases linearly with δ. The theory also predicts that above a certain value of δ, no in-sync actuation occurs. Our study aims to validate the theory and gain a deeper understanding of the motion of planar microswimmers and improve their controllability. As shown in Figure 1b, increasing the magnitude of the static field, while preserving the magnitude of the rotating field, results in a lower value of the cone angle α (or increase in δ). The magnitude of the rotational field is set to 15 mT. Using an in-plane and conically rotating field, a microswimmer that was initially located at the bottom of the chamber was set to propel upward. To reduce the hydrodynamic interaction with the boundary, the microswimmers were set to reach 1,000 μm above the bottom wall prior to being steered along an arbitrary direction by a conically rotating field. All microswimmers used in the experiments were magnetized in-plane along their symmetry axis, and the magnetization orientation was examined under a static magnetic field prior to propulsion experiments.

At frequency 12 Hz, where all δ values exhibit in-sync propulsion, the velocity is measured for δ between 0.1 and 0.3 by increasing δ by 0.02. **Figure 5**a demonstrates that as δ increases, velocity increases almost linearly.

As shown in Figure 5b, we observed a frequency band that has a constant velocity in three δ values (0.1, 0.2, and 0.3). The experimental chamber was exposed to a conically rotating field with increasing frequency from 1 Hz to 20 Hz for each δ value. Experimentally observed values of the step-in frequency, delimiting the range of in-sync actuation from below, are 1 Hz, 3 Hz, and 6 Hz for $\delta = 0.1$, 0.2, and 0.3, respectively. The value of the step-out frequency, 18 Hz, was found to be largely independent ofδ. **Table 1** provides the constant velocities and in-sync propulsion characteristics for $\delta = 0.1$, 0.2, and 0.3. At $\delta = 0.4$, only

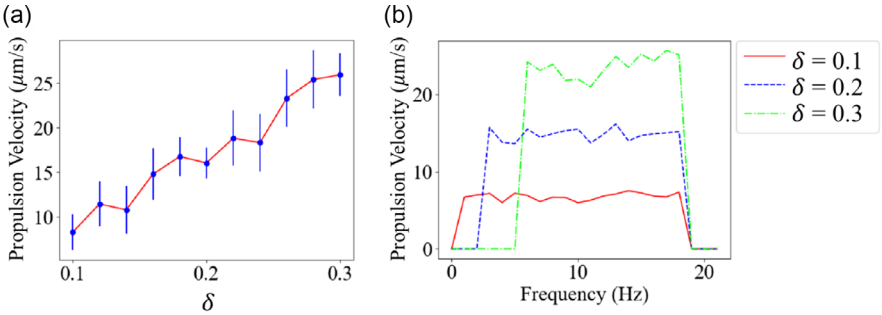

Figure 5. a) Propulsion velocity (μm s^{-1}) versus δ for in-sync actuation regime; the magnitude of the in-plane rotating field component is 15 mT. b) Propulsion velocity (μm s^{-1}) versus actuation frequency (Hz) for three different values of $\delta = 0.1$, 0.2, and 0.3.

Table 1. In-sync propulsion velocity, step-in and step-out frequencies for different δ values.

	$\delta = 0.1$	$\delta = 0.2$	$\delta = 0.3$
Propulsion speed ($\mu m\ s^{-1}$)	8.3	16.0	25.9
Step-in frequency (Hz)	1	3	6
Step-out frequency (Hz)	18	18	18

asynchronous rotation was observed regardless of actuation frequency, resulting in a relatively low propulsion velocity with a mean value of 5.41 $\mu m\ s^{-1}$ averaged over the actuation frequencies between 1 and 15 Hz in three sets of experiments. For frequencies >15 Hz, no significant propulsion was found.

2.2. Comparison with Theory

Theoretically, the dimensionless propulsion velocity corresponding to the in-sync actuation regime is given by:[36]

$$\frac{U}{\omega_0 l} = \widetilde{Ch}\frac{2\delta}{1+\varepsilon-p^{-1}} \tag{2}$$

where l is the length of the microswimmer, ω_0 is the characteristic (magnetoviscous) angular frequency, p and ε are the longitudinal and transverse rotational anisotropy parameters, respectively, and $\widetilde{Ch}$ is the dimensionless pseudochirality coefficient measuring the viscous rotation–translation coupling of the microswimmer.[36] The geometric parameters ε, p, and $\widetilde{Ch}$ are computed numerically using the bead-based multiple expansion scheme,[35] while the characteristic frequency is estimated from the experimental data as $\nu_0 = \omega_0/2\pi \cong 7.2$ Hz (see SI for details).

Figure 6b shows the comparison of the experiments with the theory in terms of scaled propulsion velocity (measuring the displacement per one revolution of the field relative to propeller's size), $U/\nu_0 l$, versus dimensionless actuation frequency, ω/ω_0 for four different values of δ. The magnetization direction and orientation of the principal rotational axes of the V-shaped microswimmer are depicted schematically in Figure 6a.

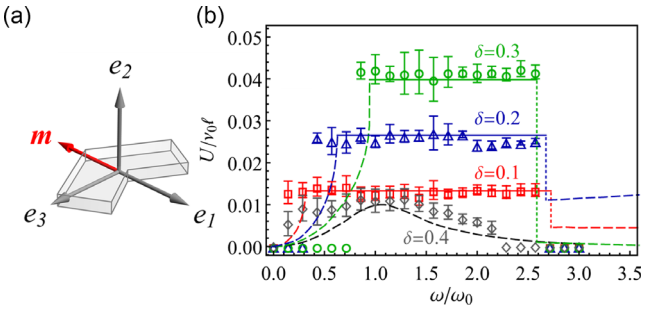

Figure 6. a) Principal rotation axes (black arrows) and the magnetic moment $\boldsymbol{m}$ (red arrow) of the V-shaped microswimmer. b) Scaled propulsion velocity of the planar microswimmer versus scaled actuation frequency. Symbols stand for the experimental results, lines to the theoretical predictions.[35] Solid and dashed lines correspond to synchronous and asynchronous rotation, respectively. Different colors represent different values of δ; the error bars represent the standard deviation.

As can be readily seen from Figure 6b, there is an excellent agreement between the theory and the experiment for all cone angles (i.e., for different values of δ). As was predicted theoretically, the V-shaped planar microswimmers magnetized along their symmetry axis exhibit unidirectional propulsion with a constant velocity in Equation (2) along the Y axis of the field rotation in a finite range of actuation frequencies limited by the step-in and the step-out frequency, respectively, $\omega_* < \omega < \omega_{s-o}$. Within this frequency range, the microswimmer rotates in-sync with the actuation field. Notice that excellent agreement with the theory was found not only for the propulsion velocity but also for the step-in and step-out frequencies. In agreement with the theory, we observe in-sync propulsion for $\delta = 0.1 - 0.3$, while for smaller cone angles ($\delta \gtrsim 0.4$) only asynchronous actuation was observed, resulting in comparatively low propulsion velocity (see Figure 6b).

2.3. Discussion

Under a conically rotating magnetic field, the planar V-shaped and in-plane magnetized microswimmers swim at a constant velocity within a limited frequency range, as demonstrated in our experiments. Such planar microstructures are easy to mass-produce and they are predisposed to in-plane magnetization, rendering them promising candidates as small-scale microswimmers. The experimental results are consistent with the theory and these experiments serve to improve our comprehension of their controllability.

Our research indicates that the velocity of microswimmers can be altered by merely adjusting the amplitude of the static field, which results in a change in the cone angle. An increase in propulsion velocity is found upon increasing the magnitude of the static field while keeping the rotating field magnitude fixed. This notion is crucial for velocity control in future research, aiding microswimmer controllability.

In addition, the constant (frequency-invariant) propulsion velocity is found within a limited frequency band, which simplifies the control of microswimmers' motion. The experiment and theory show a high degree of agreement, although minor discrepancies may arise from slight variations in the magnetization orientation and/or magnitude during manufacturing, leading to slight differences in propulsion speed among different propellers.

By effectively steering a swarm of microswimmers, we have demonstrated their potential for targeted drug delivery. Deviation in predetermined trajectories may arise due to manufacturing defects resulting in variations in magnetization. Consequently, employing a swarm of robotic microswimmers can enhance the application's success rate. A swarm of planar microswimmers can also be used in complex tasks that require swimmers to follow different trajectories due to the fact that microswimmers with different magnetizations can follow different paths in the same magnetic field. Although these results are encouraging, additional research is required to fully utilize the potential of robotic microswimmer swarms in a variety of biomedical applications. Morozov et al. proposed actuation using an asymmetric in-plane rotating field (i.e., uniform in-plane rotating field combined with a constant field acting in the same

plane) resulting in a net drift perpendicular to the field rotation axis.[38] This field-induced drift has not been yet experimentally demonstrated, but it has the potential to enhance the control capabilities of the system. In this work, an open-loop control strategy is employed. Using a closed-loop controller reduces the positional error relative to predetermined trajectories, and enables velocity control.

3. Conclusion

In conclusion, this study examines the propulsion of geometrically achiral planar microswimmers magnetized in-plane in an aqueous solution driven by a conically rotating magnetic field. Experimental findings confirm the theoretical predictions and demonstrate that these microswimmers exhibit unidirectional propulsion motion in the bulk fluid within a limited range of actuation frequencies. The propulsion speed is independent of the actuation frequency and controlled by the cone angle of the field. Although these microswimmers can be mass-produced by low-cost photolithography techniques and they can be easily magnetized in-plane, the major obstacle to their use was the lack of controllability, as they typically exhibit bidirectional propulsion when driven by an in-plane rotating magnetic field. In this work, we demonstrate that adding the constant magnetic field along the field rotation axis (i.e., applying a conically rotating field) results in the selection of the propulsion direction.

Our findings suggest that planar magnetic microswimmers hold promise as potential candidates for the future in vivo biomedical applications, such as drug delivery. The present work experimentally demonstrates the controllability of propulsion for both individual and multiple in-plane magnetized planar microswimmers.

4. Experimental Section

Fabrication of V-Shaped Planar Microswimmers: Planar microswimmers are manufactured via conventional photolithography technology, as illustrated in **Figure 7**. First, a silicon wafer is coated with a dextran sacrificial layer. Dextran is utilized because it is water-soluble. The SU-8 2005 photoresist is then spin-coated onto the dextran sacrificial layer, as shown in Figure 7a. As depicted in Figure 7b, V-shaped structures can be acquired using standard photolithography steps such as soft bake, exposure, and postexposure bake. The wafer is then treated with oxygen plasma to eliminate the dextran layer, as depicted in Figure 7c, so that the microswimmers are not released together with the coated nickel in the following phase. As demonstrated in Figure 7d, a thin nickel coating (100 nm) is deposited

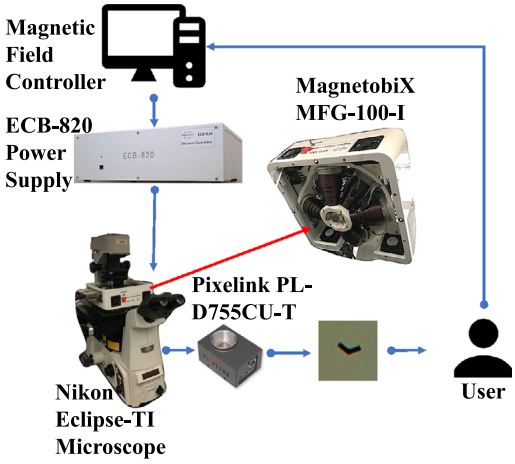

Figure 8. Nikon Eclipse-TI microscope is used for the experiments. MagnetobiX MFG-100-I magnetic field generator is used to generate a conically rotating magnetic field. The magnetic field is controlled with MBX PRO software and an ECB-820 power supply. Pixelink PL-D755CU-T camera is used to capture the images.

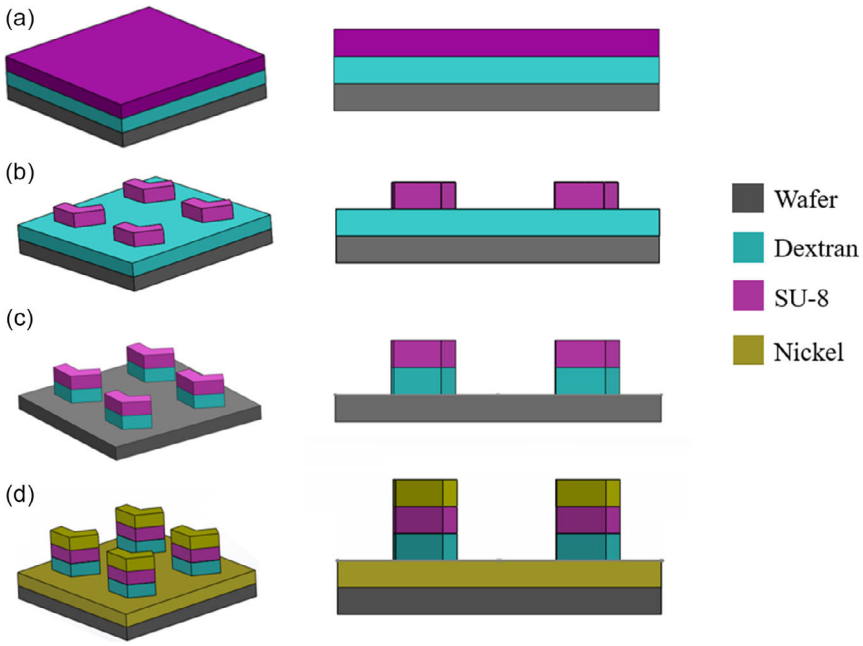

Figure 7. Perspective and side views of manufacturing steps: a) dextran and SU-8 coating, b) exposure, c) dextran removal, and d) nickel coating.

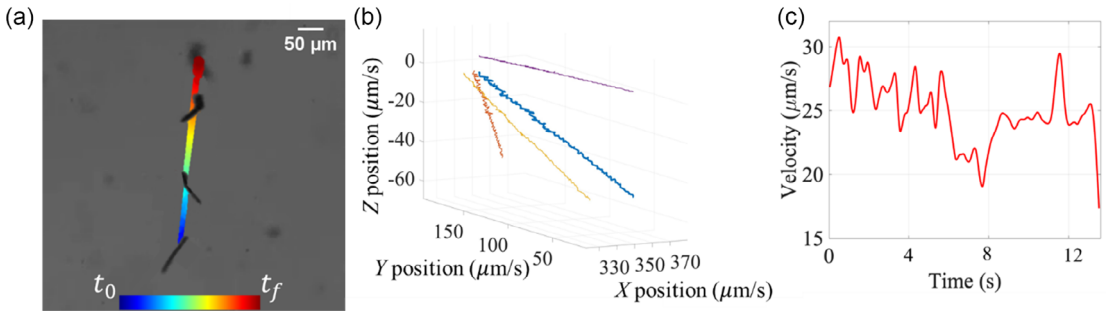

Figure 9. a) 2D trajectory of single planar microswimmer under a conically rotating magnetic field (δ=0.3). b) Motion in 3D (μm). The blue line shows the 3D position of the microswimmer; purple, orange, and yellow lines are the projections of the trajectory onto the *XY*, *XZ*, and *YZ* planes, respectively. c) The velocity of the microswimmer versus time throughout the experiment.

using electron-beam evaporation on the SU-8 structures to impart magnetic properties to the microswimmers. By submerging the sample in water, microswimmers were released for experiments.

As a result of plasma etching removing the superfluous dextran, the nickel surrounding the microswimmers will not be released, allowing the microswimmers to be suspended in a debris-free environment during the experiment.

Experimental Setup: The schematics of the experimental setup are shown in **Figure 8**. To prevent fluid leakage, a 10 mm-diameter PDMS chamber was placed over the cover glass (No. 1, 22 mm × 30 mm). Similarly, an additional top glass was used to avoid evaporation, dust accumulation, and internal flow. The bottom of the chamber was coated with a 20% Tween20 (Sigma-Aldrich) solution to prevent microswimmers' adhesion to the glass substrate. Then, a 20% NaCl solution was added to the chamber. The planar microswimmers fabricated by photolithography were then deployed inside the PDMS chamber. Photolithography was used to fabricate microswimmers, as discussed in detail in the prior work.[40] For visualization, we employed the Nikon Eclipse-TI Microscope equipped with a 10x objective lens. However, to capture the entire experimental chamber in the video in the Supporting Information corresponding to Figure 4b, we opted for 2x objective lens. Using the Pixelink PL-D755CU-T camera, experimental videos were recorded.

MagnetobiX AG (Switzerland) MFG-100-I, a commercially available magnetic field generator, was utilized to control the motion of planar microswimmers during the experiments. MFG-100-I can create gradient-free uniform fields, making it an ideal option for our problem formulation. A magnetic field generator capable of simultaneously producing static and rotating fields with its eight electromagnetic coils was applied to generate a conically rotating magnetic field. During the experiments, an open-loop control method was utilized. The magnetic field was preprogrammed using the software interface of the magnetic field generator.

Position Tracking in 3D: As the distance between microswimmers and the focal plane increases, the image becomes blurry. To track the movement of the microswimmers along the *Z*-axis, we developed an image-processing algorithm that measures the blurriness level. Fast Fourier transform (FFT) was applied to each image. Then, we reset the center of our FFT to zero. Then, the inverse shift was applied to place the DC component (image mean) back in the top-left position, followed by the inverse FFT. We recomputed the magnitude spectrum of the reconstructed image after the center DC values had been zeroed. Next, the mean of the magnitude value was computed. The magnitude mean of an image is inversely proportional to its blurriness. This indicates that this value is inversely proportional to the distance between the microswimmer and the focal plane. To track microswimmers in *Z*-axis in micrometers, the focal plane of a planar microswimmer was altered under specific camera resolution and lighting conditions to capture images. The position of the focal plane was recorded during image capture. Then, we calculated the distance between the focal plane and the microswimmer by scaling the above-described magnitude mean image to micrometers. Position in *XY*-plane (in 2D) was tracked with ordinary binary image processing. The pixel-to-micrometer ratio was calculated with the help of a high-precision ocular calibration ruler. The distance calculated in pixels was converted to micrometers. Instant velocity throughout the experiment was calculated using position and time. Due to the microswimmer's V-shaped design, the location data contain a minor amount of noise, which is reduced using a Kalman Filter while computing the instant velocity. A result is demonstrated in **Figure 9**. Figure 9a shows the 2D tracking of a microswimmer while Figure 9b demonstrates the 3D tracking using the aforementioned method. The experiment was conducted for $\delta = 0.3$ (static field of 4.5 mT). The velocity versus time of the experiment is shown in Figure 9c.

Supporting Information

Supporting Information is available from the Wiley Online Library or from the author.

Acknowledgements

This work was financially supported by the United States–Israel Binational Science Foundation (#2021657), the National Science Foundation (CMMI #2123824), the Guangdong Basic and Applied Basic Research Foundation (2023A1515012229), the Department of Education of Guangdong (2021ZDZX2037), and the Science and Technology Innovation Committee Foundation of Shenzhen (RCYX20210609103644015). The authors acknowledge the technical support provided by the SUSTech Core Research Facilities (SCRF) for the fabrication of V-shaped microswimmers, as well as the insightful discussion and proofreading assistance provided by Benjamin Kuo.

Conflict of Interest

The authors declare no conflict of interest.

Data Availability Statement

The data that support the findings of this study are available in the supplementary material of this article.

Keywords

low-Reynolds-number flows, magnetic control, microswimmers, propulsion

Received: September 18, 2023
Revised: October 29, 2023
Published online: November 12, 2023

[1] K. Bente, A. Codutti, F. Bachmann, D. Faivre, *Small* **2018**, *14*, 1704374.
[2] G. Kararsiz, Y. C. Duygu, L. W. Rogowski, A. Bhattacharjee, M. J. Kim, *Micromachines* **2022**, *13*, 1005.
[3] W. Jing, D. Cappelleri, *Robotics* **2014**, *3*, 106.
[4] A. Ferreira, J. Agnus, N. Chaillet, J. M. Breguet, *IEEE/ASME Trans. Mechatron.* **2004**, *9*, 508.
[5] H. Wang, M. Pumera, *Adv. Funct. Mater.* **2018**, *28*, 1705421.
[6] A. Credi, *Angew. Chem., Int. Ed.* **2014**, *53*, 4274.
[7] L. W. Rogowski, X. Zhang, J. Tang, M. Oxner, M. J. Kim, *Biomicrofluidics* **2021**, *15*, 044104.
[8] C. H. Chiou, Y. Y. Huang, M. H. Chiang, H. H. Lee, G. Bin Lee, *Nanotechnology* **2006**, *17*, 1217.
[9] X. Zhang, H. Kim, M. J. Kim, *IEEE Trans. Instrum. Meas.* **2019**, *68*, 680.
[10] B. J. Nelson, I. K. Kaliakatsos, J. J. Abbott, *Annu. Rev. Biomed. Eng.* **2010**, *12*, 55.
[11] E. M. Purcell, *Am. J. Phys.* **1977**, *45*, 3.
[12] U. K. Cheang, D. Roy, J. H. Lee, M. J. Kim, *Appl. Phys. Lett.* **2010**, *97*, 213704.
[13] J. Ali, U. K. Cheang, J. D. Martindale, M. Jabbarzadeh, H. C. Fu, M. Jun Kim, *Sci. Rep.* **2017**, *7*, 14098.
[14] O. Felfoul, M. Mohammadi, S. Taherkhani, D. De Lanauze, Y. Zhong Xu, D. Loghin, S. Essa, S. Jancik, D. Houle, M. Lafleur, L. Gaboury, M. Tabrizian, N. Kaou, M. Atkin, T. Vuong, G. Batist, N. Beauchemin, D. Radzioch, S. Martel, *Nat. Nanotechnol.* **2016**, *11*, 941.
[15] X. Yan, Q. Zhou, M. Vincent, Y. Deng, J. Yu, J. Xu, T. Xu, T. Tang, L. Bian, Y.-X. J. Wang, K. Kostarelos, L. Zhang, *Sci. Rob.* **2017**, *2*, 22.
[16] B. E. F. De Ávila, P. Angsantikul, J. Li, M. Angel Lopez-Ramirez, D. E. Ramírez-Herrera, S. Thamphiwatana, C. Chen, J. Delezuk, R. Samakapiruk, V. Ramez, L. Zhang, J. Wang, *Nat. Commun.* **2017**, *8*, 272.
[17] U. Kei Cheang, K. Lee, A. A. Julius, M. J. Kim, *Appl. Phys. Lett.* **2014**, *105*, 083705.
[18] B. J. Nelson, K. E. Peyer, *ACS Nano* **2014**, *8*, 8718.
[19] M. A. Zeeshan, R. Grisch, E. Pellicer, K. M. Sivaraman, K. E. Peyer, J. Sort, B. Özkale, M. S. Sakar, B. J. Nelson, S. Pané, *Small* **2014**, *10*, 1284.
[20] L. Zhang, J. J. Abbott, L. Dong, B. E. Kratochvil, D. Bell, B. J. Nelson, *Appl. Phys. Lett.* **2009**, *94*, 064107.
[21] X. Yan, Q. Zhou, J. Yu, T. Xu, Y. Deng, T. Tang, Q. Feng, L. Bian, Y. Zhang, A. Ferreira, L. Zhang, *Adv. Funct. Mater.* **2015**, *25*, 5333.
[22] D. Walker, M. Kübler, K. I. Morozov, P. Fischer, A. M. Leshansky, *Nano Lett.* **2015**, *15*, 4412.
[23] E. J. Smith, D. Makarov, S. Sanchez, V. M. Fomin, O. G. Schmidt, *Phys. Rev. Lett.* **2011**, *107*, 097204.
[24] W. Gao, X. Feng, A. Pei, C. R. Kane, R. Tam, C. Hennessy, J. Wang, *Nano Lett.* **2014**, *14*, 305.
[25] C. Peters, O. Ergeneman, P. D. W. García, M. Müller, S. Pané, B. J. Nelson, C. Hierold, *Adv. Funct. Mater.* **2014**, *24*, 5269.
[26] Y. Yu, L. Shang, W. Gao, Z. Zhao, H. Wang, Y. Zhao, *Angew. Chem., Int. Ed.* **2017**, *56*, 12127.
[27] Y. Mirzae, O. Dubrovski, O. Kenneth, K. I. Morozov, A. M. Leshansky, *Sci. Rob.* **2018**, *15*, 4412.
[28] U. K. Cheang, F. Meshkati, D. Kim, M. J. Kim, H. C. Fu, *Phys. Rev. E* **2014**, *90*, 033007.
[29] K. I. Morozov, Y. Mirzae, O. Kenneth, A. M. Leshansky, *Phys. Rev. Fluids* **2017**, *2*, 044202.
[30] J. Sachs, K. I. Morozov, O. Kenneth, T. Qiu, N. Segreto, P. Fischer, A. M. Leshansky, *Phys. Rev. E* **2018**, *98*, 063105.
[31] L. W. Rogowski, J. Ali, X. Zhang, J. N. Wilking, H. C. Fu, M. J. Kim, *Nat. Commun.* **2021**, *12*, 1116.
[32] L. W. Rogowski, M. J. Kim, *Sci. Rep.* **2022**, *12*, 17646.
[33] X. Song, W. Fu, U. K. Cheang, *iScience* **2022**, *25*, 104507.
[34] X. Mu, Y. Zhong, T. Jiang, U. K. Cheang, *Mater. Adv.* **2021**, *2*, 3871.
[35] K. J. Cohen, B. Y. Rubinstein, O. Kenneth, A. M. Leshansky, *Phys. Rev. Appl.* **2019**, *12*, 014025.
[36] S. Tottori, B. J. Nelson, *Small* **2018**, *14*, 1800722.
[37] S. Kim, S. J. Karrila, *Microhydrodynamics: Principles and Selected Applications*, Butterworth-Heinemann, Boston, MA **1991**.
[38] K. I. Morozov, A. M. Leshansky, *Phys. Chem. Chem. Phys.* **2020**, *22*, 16407.
[39] J. Giltinan, P. Katsamba, W. Wang, E. Lauga, M. Sitti, *Appl. Phys. Lett.* **2020**, *116*, 134101.
[40] Z. Chen, Z. Wang, D. Quashie, P. Benhal, J. Ali, M. J. Kim, U. K. Cheang, *Sci. Rep.* **2021**, *11*, 21190.